Eur. J. Mineral.
2018, **30**, 149–164
Published online 27 February 2018

The crystal structures of heptasartorite, $Tl_7Pb_{22}As_{55}S_{108}$, and enneasartorite, $Tl_6Pb_{32}As_{70}S_{140}$, two members of an anion-omission series of complex sulfosalts from Lengenbach, the Swiss Alps, and comparison with the structures of As–Sb sartorite homologues

EMIL MAKOVICKY[1,*], DAN TOPA[2] and BERTHOLD STOEGER[3]

[1] Department of Geoscience and Resource Management, University of Copenhagen, Østervoldgade 10, 1350 Copenhagen K, Denmark
*Corresponding author, e-mail: emilm@geo.ku.dk
[2] Naturhistorisches Museum, Burgring 7, 1010 Wien, Austria
[3] Technische Universität Wien, Karlsplatz 13, 1040 Wien, Austria

Abstract: Crystal structures of heptasartorite and enneasartorite, two members of the sartorite anion-omission series were refined from the material from the Lengenbach deposit, Swiss Alps. Heptasartorite, $Tl_7Pb_{22}(As_{54}Sb)_{\Sigma 55}S_{108}$, is monoclinic, space group: $P2_1/c$ (SG#14), a 29.2691(20), b 7.8768(5), c 20.1275(15) Å, β 102.065(2)°, unit-cell volume $V = 4537.8(5)$ Å^3. Enneasartorite, $Tl_6Pb_{32}As_{70}S_{140}$, is monoclinic, space group $P2_1/c$ (SG#14), and lattice parameters $a = 37.612(6)$, $b = 7.8777(12)$, $c = 20.071(3)$ Å, $\beta = 101.930(2)°$, and $V = 5818.6(15)$ Å^3. Both structures are typical structures of an $N = 3$ homologue of the sartorite homologous series with zig-zag walls of (Pb, Tl) trigonal coordination prisms separating (primarily) As-based slabs of structure configured to accommodate lone electron pairs of As. The sevenfold superstructure of heptasartorite is based on a sequence of crankshaft chains: on a surface of a fundamental double-ribbon in the As-rich structure slab one can recognize a W-shaped chain with five As and one mixed coordination polyhedron in which As and a large cation combine, a 4-member chain, a pair of As polyhedra, and two isolated As polyhedra. In the here redetermined structure of enneasartorite, one more 4-member chain of As polyhedra has been added, making the environment of the W-shaped chain symmetric. One of the isolated As polyhedra became a mixed-cation site. In both structures, the S site chelated by the As atoms of the W chain becomes vacant, generating the anion-omission derivatives of the ideal $PbAs_2S_4$ motif. The chain motifs differ from those in the Sb–As homologues of sartorite, which display only two-fold superstructures.

Key-words: crystal structure; heptasartorite; enneasartorite; sartorite homologous series; anion-omission series; Pb–Tl–As sulfosalts; Tl substitution.

1. Introduction

Sartorite was described in 1868 and named after Sartorius von Waltershausen, a German mineralogist. The classical crystal structure determination by Iitaka & Nowacki (1961), was performed only on a substructure. It was known at that time that sartorite displays a faint superstructure on single-crystal X-ray diffraction photographs. This was estimated as a 20-tuple of the fundamental 4.2 Å period by Bannister *et al.* (1939) and Berry (1940), and as a 11-tuple by Nowacki *et al.* (1963); the 19.6 Å period was found to be tripled although Berry (1940) finds it quadrupled.

Iitaka & Nowacki (1961) solved and refined the sartorite structure *on a subcell level* with the monoclinic space group $P2_1/n$, $a = 19.62$, $b = 7.89$, $c = 4.19$ Å, $\alpha = \beta = \gamma = 90°$ and Nowacki *et al.* (1961) specified the true cell of sartorite as a commensurate superstructure with $3 \times a = 58.8$, $b = 7.89$, $11 \times c = 46.1$ Å and space group $P2_1/n$, but were not able to resolve it. Nowacki *et al.* (1963) state, however, that the $3 \times 1 \times 11$ true cell is not always present and "satellite reflections may occur instead in the X-ray diffraction photographs". Electron diffraction studies, performed by Pring *et al.* (1993) on Lengenbach sartorite, showed satellite reflections that were generally incommensurate with respect to the subcell $a = 19.62$, $b = 7.89$, $c = 4.19$ Å, $\beta = 90°$ and space group $P2_1/n$. From electron diffraction data on unspecified Lengenbach sartorite, Pring (2001) gives a modulation vector 6/13(101)* for the same lattice. Data on true symmetry of sartorite varied widely as well.

It might be worth mentioning that the mixed arsenic-antimony $N = 3$ sartorite homologues, twinnite $Pb_{0.8}Tl_{0.1}Sb_{1.3}As_{0.8}S_4$, space group $P2_1/n$ (Makovicky

https://doi.org/10.1127/ejm/2018/0030-2706
0935-1221/18/0030-2706 $ 7.20

& Topa, 2012) and guettardite, $PbAsSbS_4$, space group $P2_1/c$ (Makovicky *et al.*, 2012), have simple 8.5–8.6 Å periods, without modulation. Apparently, greater length of Sb–S bonds and a different lone electron pair stereoactivity of antimony eliminate the need for complicated superstructures which are present in arsenic-based $N=3$ structures.

In the detailed electron microprobe investigation of the Lengenbach material, Laroussi *et al.* (1989) could not find a phase corresponding to the ideal sartorite, $PbAs_2S_4$, expected by Iitaka and Nowacki (1961) on the basis of the substructure determination. Furthermore, Nowacki & Bahezre (1963), Laroussi *et al.* (1989) and Berlepsch *et al.* (2003) showed that sartorite can contain variable amounts of Tl (from 2.6 to 6.5%Tl, respectively).

The explanation for this strange behavior was supplied by the results of Berlepsch *et al.* (2003) obtained on "sartorite with a ninefold superstructure". Berlepsch *et al.* (2003) solved and refined a commensurate ninefold sartorite superstructure with space group $P2_1/c$; $a=37.71(2)$, $b=7.898(3)$, $c=20.106(8)$ Å, $\beta=101.993(7)^\circ$ and with the empirical formula $Pb_{8.2}Tl_{1.4}As_{17.5}Sb_{0.5}S_{35}$. The refined formula $Pb_8Tl_{1.5}As_{17.5}S_{35}$, with one ordered sulfur vacancy, is in a good agreement. This phase has a high Tl content, up to 6.5 wt% and the authors suggest that the incorporation of substantial amounts of Tl^+ into $PbAs_2S_4$ is essential for the type and periodicity of superstructures in sartorite.

Clarification of the chemistry and crystal structure of various "sartorite" specimens required extensive study which revealed that we do not deal with varieties of one mineral species but with a family of closely related but *structurally and chemically distinct minerals*. When talking collectively about all these phases, we shall use the term "M-sartorites" (M is equal to 7, 9, and/or 11) instead of enumerating them again and again. This paper deals with the 7- and 9-fold derivatives, a detailed treatment for the 11-fold derivative, hendekasartorite (Topa *et al.*, 2015, 2017) is in preparation.

Based on fundamental structural properties derived from the structure determinations by the Nowacki group (publications in the years 1961–1970) and Le Bihan (1962), Makovicky (1985) defined a *sartorite homologous series* of Pb–As and Pb–As–Sb sulfosalts with a set of common structural features and principles, and with sartorite as its lowermost member. The definition of the series, based on the most fundamental principles persisted well through all incremental changes in its volume and contents, which were brought about by new mineral phases, and was helpful in the ongoing research. The elucidation of the fine structure of the "sartorite" species is one more enrichment and refinement of the series and the new minerals derived from the original "sartorite" form a series of *anion-omission derivatives* within the $N=3$ homologues of the sartorite homologous series. The fact that we predicted some of these structures already in the paper by Berlepsch *et al.* (2003), long before appropriate material was found, is one more example to illustrate the power of modular crystallography.

2. Experimental procedure

Chemical composition of the structurally analyzed material was obtained by electron microprobe analyses specified in detail in Topa *et al.* (2017). The single-crystal data from diffractometer measurements specified below were refined to yield cell parameters as follows.

Heptasartorite is monoclinic, space group: $P2_1/c$ (SG#14), a 29.2691(20), b 7.8768(5), c 20.1275(15) Å, β 102.065(2)°, unit-cell volume $V=4537.8(5)$ Å^3; $Z=1$ for the formula $Tl_{7.30}Pb_{21.55}(As_{53.94}Sb_{1.31})_{\Sigma 55.25}S_{107.90}$ (ΣMe = 84.1). The crystal-structure formula is $(Pb,Tl)_{\Sigma 28.8}As_{55.2}S_{108}$ (ΣMe = 84) whereas the simplified formula, $Tl_7Pb_{22}(As_{54}Sb)_{\Sigma 55}S_{108}$, was derived from the 7-fold superstructure of "ideal sartorite" (*i.e.*, $7\times Pb_4As_8S_{16}=Pb_{28}As_{56}S_{112}$). Habitus prismatic; no observable twinning. The a:b:c ratio calculated from the unit-cell parameters is 3.7159:1:2.5554.

Enneasartorite is monoclinic, space group $P2_1/c$ (SG#14), and lattice parameters $a=37.612(6)$, $b=7.8777(12)$, $c=20.071(3)$ Å, $\beta=101.930(2)^\circ$, and $V=5818.6(15)$ Å^3. The empirical formula (based on 248 *apfu*, 108Me + 140S; $Z=1$) is: $Tl_{6.42}Pb_{31.68}(As_{68.31}Sb_{1.59})_{\Sigma 69.9}S_{140.0}$ (ΣMe = 107.99). The crystal-structure formula is $(Pb,Tl)_{\Sigma 40.4}As_{67.6}S_{140}$ (ΣMe = 108) and the simplified formula, $Tl_6Pb_{32}As_{70}S_{140}$ is derived from the 9-fold superstructure of "ideal" formula of "sartorite" (*i.e.*, $9\times Pb_4As_8S_{16}=Pb_{36}As_{72}S_{144}$). Grains are prismatic without observable twinning. The a:b:c ratio was calculated from the unit-cell parameters and it is 4.77449:1:2.5478.

The derivative with 11-fold superstructure, closest to the phase which was proposed by Nowacki *et al.* (1960) based solely on X-ray diffraction photographs, was described in detail and defined as *hendekasartorite* (Topa *et al.*, 2015, 2017).

For each mineral species, a fragment with irregular shape and size specified in Tables 1 and 5 was mounted on a Bruker AXS three-circle diffractometer equipped with a CCD area detector. The SMART (Bruker, 1998a) system of programs was used for unit-cell determination and data collection, SAINT+ (Bruker, 1998b) for the reduction of the intensity data, and XPREP (Bruker, 1997) for space group determination and empirical absorption correction based on pseudo ψ-scans. The centrosymmetric space group $P2_1/c$ was proposed by the XPREP program for all three phases and was accepted. The structures were solved by direct methods (*SHELXS97,* Sheldrick, 2008), which revealed most of the atom positions. In subsequent cycles of the refinement (*SHELXL97*, Sheldrick, 2008), remaining atom positions were deduced from difference Fourier syntheses by selecting from among the strongest maxima at appropriate distances. Parameters describing data collection and refinement for the two analyzed phases are presented in Tables 1 and 5. Crystal structure refinement of heptasartorite ended at $R_1=0.0522$ for 6926 reflections with $F_o>4\sigma(F_o)$ and 0.0925 for all 10913 reflections;

Table 1. Crystal data and summary of parameters describing data collection and refinement for heptasartorite.

Crystal data			
Chemical formula	$Tl_7Pb_{22}As_{55}S_{108}$	Unit-cell parameters	
Crystal system	Monoclinic	a(Å)	29.269(2)
Space group	$P2_1/c$ (#14)	b(Å)	7.8768(5)
D_x (mg m^{-3})	*4.9*	c(Å)	20.1275(15)
No. of reflections for cell param.	5665	β(°)	102.065(2)
μ (mm^{-1})	37.02	V(Å^3)	4537.8(5)
Crystal form	Irregular	Z	1
Crystal size (mm)	0.09 × 0.08 × 0.05	Crystal color	Gray metallic

Data collection	
T_{min}, T_{max}	0.34, 0.75
No. of measured reflections	107119
No. of independent reflections	10913
No. of observed reflections	6926
Criterion for observed reflections	$I > 2\sigma(I)$
R_{int} (%), $R_{(sigma)}$ (%)	12.03, 7.49
θ_{max}(°)	27.99
Range of h, k, l	$-38 \le h \le 38$, $-10 \le k \le 10$, $-26 \le l \le 26$

Refinement on F_o^2	
$R[F_o>4\sigma(F_o)]$ (%)	5.22
$wR(F_o^2)$ (%)	9.25
S*(GooF)*	1.051
No. of reflections used in refinement	6926
No. of parameters refined	444
Weighting scheme	$a=0.03$, $b=92$ $w = 1/[\sigma^2(F_o^2) + (aP)^2 + bP]$where $P = (F_o^2 + 2F_c^2)/3$
$(\Delta/\sigma)_{max}$	0.002
$\Delta\rho_{max}$ (e/Å^3)	5.32(0.86 Å from As14)
$\Delta\rho_{min}$ (e/Å^3)	−2.71 (0.67 Å from As14)
Extinction coefficient	None
Source of atomic scattering factors	*International Tables for X-Ray Crystallography* (1992, Vol. C, Tables 4.2.6.8 and 6.1.1.4)

wR2 is 11.91%. Crystal structure refinement of enneasartorite was terminated at $R_1 = 0.0646$ for 5862 reflections with $F_o > 4\sigma(F_o)$ and 0.0933 for all 8301 data.

3. Crystal structures

Coordinates, occupancy factors and equivalent isotropic displacement parameters of atoms in the examined mineral structures are given in Tables 2 and 6, respectively for heptasartorite and enneasartorite, selected interatomic distances (Å) in Tables 3 and 7, and polyhedron characteristics for cations in Tables 4 and 8. Anisotropic displacement parameters can be requested from the first author.

Heptasartorite. The structure of heptasartorite contains 21 independent metal and 27 distinct sulfur sites in the asymmetric unit. There are six (predominantly) Pb sites, one predominantly Tl site, 13 As sites, and one mixed (As, Pb) site with ~20% Pb (see Table 2). The Tl content in the heavy-atom sites is estimated from cation-sulfur distances (Table 3) and bond-valence sum (Table 4).

The unit cell of heptasartorite is a sevenfold supercell of the "fundamental 4.2 Å cell" of the sartorite homologous series for the homologue $N=3$. The a parameter is seven times 4.2 Å, whereas the b and c parameters are typical parameters for the known $N=3$ homologues (guettardite and twinnite) (Figs. 1 and 2, Table 9).

The nominal lead atoms, Pb1 to Pb7, are arranged in [1 0 0] columns of tricapped trigonal coordination prisms, except for the Pb2 site which has *one of the capping sulfurs missing* (namely the sulfur atom which should be embedded in a S column parallel to a and situated between S14 and S17, *i.e.*, between As9 and As12). Three of the nominally lead positions, Me4, and to a lesser extent the Me1 and the Me6 position, have inflated coordination polyhedra, respectively suggesting mixed (Tl, Pb) and (Pb, Tl) occupancies.

Replacement of Pb by Tl in this Tl-richest "M-sartorite" species has been modeled using volume of a sphere circumscribed to the (Pb, Tl) tricapped trigonal prism. For comparison, prisms with small volumes, presumed to contain pure Pb were chosen: Pb2, 3, and 5 in heptasartorite (average volume 128.71 Å^3) and five such prisms from hendekasartorite (Topa *et al.*, 2017) with the average volume 131.79 Å^3. The grand average 130.25 Å^3 was used and contrasted with the average volume of (presumably) pure Tl prisms of this kind from parapierrotite (161.17 Å^3) and pierrotite (156.11 Å^3 and 163.11 Å^3), which give a grand average of 160.13 Å^3.

Table 2. Coordinates, occupancy factors and equivalent isotropic displacement parameters (in Å^2) of atoms in heptasartorite.

Atom	Label	sof	x	y	z	U_{eq}
Pb1	Pb/Tl		0.28130(2)	0.40872(8)	0.20788(3)	0.02557(15)
Pb2	Pb		0.42101(2)	0.35156(8)	0.18487(3)	0.02890(16)
Pb3	Pb		0.13666(2)	0.41870(8)	0.20994(3)	0.02699(15)
Me4	Tl/Pb		0.99127(2)	0.44679(8)	0.19343(3)	0.03030(16)
Pb5	Pb		0.70406(2)	0.40266(9)	0.18579(3)	0.02931(16)
Pb6	Pb/Tl		0.56254(2)	0.40854(8)	0.18847(3)	0.02906(16)
Pb7	Pb/Tl		0.15121(3)	0.92043(10)	0.30463(4)	0.04169(19)
As1	As	0.802(4)	0.67538(5)	0.69682(17)	0.00944(7)	0.0318(5)
Pb8	Pb	0.198(4)	0.67538(5)	0.69682(17)	0.00944(7)	0.0318(5)
As2	As		0.04308(5)	0.33765(19)	0.00071(7)	0.0173(3)
As3	As		0.08777(5)	0.53290(19)	0.36795(7)	0.0173(3)
As4	As		0.03917(5)	0.00480(19)	0.12061(7)	0.0176(3)
As5	As		0.74705(5)	0.3153(2)	0.00701(7)	0.0189(3)
As6	As		0.19888(5)	0.01268(19)	0.13504(7)	0.0179(3)
As7	As		0.37531(5)	0.4985(2)	0.36283(8)	0.0213(3)
As8	As		0.12092(6)	0.6904(2)	0.03859(9)	0.0275(4)
As9	As		0.49694(5)	−0.0316(2)	0.13278(8)	0.0220(3)
As10	As		0.45630(6)	0.2868(2)	0.00901(8)	0.0250(4)
As11	As		0.15891(5)	0.3148(2)	−0.01355(8)	0.0218(3)
As12	As		0.32081(6)	−0.01729(19)	0.11864(8)	0.0217(3)
As13	As		0.76614(6)	−0.00776(19)	0.11387(8)	0.0233(4)
As14	As		0.39687(6)	0.6716(2)	0.01908(9)	0.0289(4)
S1	S		0.06644(13)	0.1488(5)	0.21663(18)	0.0186(8)
S2	S		0.77908(13)	0.1288(5)	0.21451(18)	0.0181(8)
S3	S		0.35071(13)	0.1235(5)	0.21533(18)	0.0206(8)
S4	S		0.14602(13)	−0.1704(5)	0.15944(18)	0.0185(8)
S5	S		0.38198(13)	0.5130(5)	−0.07344(19)	0.0220(8)
S6	S		0.18260(13)	0.5060(5)	0.07613(18)	0.0186(8)
S7	S		0.07650(13)	0.6701(5)	0.2674(2)	0.0222(8)
S8	S		0.34431(13)	0.5345(5)	0.07419(18)	0.0202(8)
S9	S		0.13945(13)	0.3385(5)	0.34789(18)	0.0179(8)
S10	S		0.21329(13)	0.1548(5)	0.2346(2)	0.0209(8)
S11	S		0.10776(13)	0.5070(5)	−0.06945(18)	0.0204(8)
S12	S		0.35976(14)	0.6471(5)	0.2664(2)	0.0288(10)
S13	S		0.31502(13)	0.3187(5)	0.34230(18)	0.0192(8)
S14	S		0.26285(13)	−0.1668(5)	0.15630(19)	0.0195(8)
S15	S		0.69934(13)	0.1524(5)	0.05932(19)	0.0210(8)
S16	S		0.81115(13)	0.1642(5)	0.05892(19)	0.0220(8)
S17	S		0.43314(13)	0.3202(4)	0.33810(19)	0.0192(8)
S18	S		0.49943(14)	0.1206(5)	0.2274(2)	0.0260(9)
S19	S		0.02258(13)	0.3581(4)	0.34873(18)	0.0176(8)
S20	S		0.46720(14)	0.5314(5)	0.0737(2)	0.0244(9)
S21	S		0.52584(14)	0.1563(5)	0.06577(19)	0.0242(9)
S22	S		0.06357(13)	0.5499(5)	0.08264(18)	0.0199(8)
S23	S		0.10396(13)	0.1601(5)	0.0327(2)	0.0232(8)
S24	S		0.40605(15)	0.1409(5)	0.0596(2)	0.0296(10)
S25	S		0.75426(15)	0.5438(5)	0.0765(2)	0.0268(9)
S26	S		−0.00811(13)	0.1986(5)	0.0543(2)	0.0226(8)
S27	S		0.27337(16)	0.1849(5)	0.0624(2)	0.0331(10)

Then the volume of a sphere circumscribed to a mixed (Tl, Pb) prism can be predicted as

$$V_S = 160.13 \times \text{mol. prop. Tl} + 130.25 \times \text{mol. prop. Pb}(i.e., 1 - \text{mol. prop. Tl}).$$

Solving this equation gave 30.1 at% Tl for the Pb1 site, 58.3 at% Tl for the Pb4 site, 25.1 at% Tl for the Pb6 site, and 21.5 at% Tl for the Pb7 site. This accounts for 63.4% of Tl *pfu* found by electron microprobe analysis. If we assume that the structurally analyzed fragment had the Tl content as determined by the microprobe analysis of the aggregate, the remaining 36.6% Tl have to be distributed over the rest of cation positions, *e.g.* Pb5 and As/Pb1, or our estimates are too low. Uncertainty of the method, however, is appreciable (the polyhedron volume is not the only criterion of occupancy), and the results of this procedure must be considered as semiquantitative. When we deal with elements which have very different polyhedron radii and different R_0 and N values (Brown,

Table 3. Selected interatomic distances (Å) in heptasartorite.

Pb1–		Pb2–		Pb3–		*Me4*–	
S13	2.771(4)	S3	2.892(4)	S9	2.832(4)	S19	3.147(4)
S10	2.950(4)	S18	2.914(4)	S1	2.980(4)	S1	3.153(4)
S12	3.009(4)	S24	2.973(4)	S10	3.022(4)	S7	3.156(4)
S3	3.012(4)	S17	3.040(4)	S7	3.035(4)	S7	3.159(4)
S2	3.118(4)	S8	3.160(4)	S2	3.093(4)	S1	3.184(4)
S27	3.384(4)	S20	3.179(4)	S22	3.149(3)	S19	3.352(3)
S14	3.509(4)	S18	3.363(4)	S6	3.324(4)	S26	3.418(4)
S6	3.572(3)	S12	3.543(4)	S4	3.421(4)	S11	3.426(3)
S8	3.701(4)					S22	3.476(4)
Pb5–		Pb6–		Pb7–		As1–	
S12	3.036(4)	S12	3.062(4)	S7	2.923(4)	S8	2.466(4)
S2	3.046(4)	S18	3.127(4)	S4	2.982(4)	S27	2.473(5)
S5	3.085(3)	S5	3.155(4)	S11	3.117(4)	S25	2.702(4)
S25	3.096(5)	S21	3.177(4)	S10	3.125(4)	S24	2.804(4)
S14	3.171(4)	S18	3.199(4)	S2	3.149(4)	S5	2.848(4)
S15	3.200(4)	S17	3.293(3)	S1	3.270(4)		
S10	3.278(4)	S3	3.318(4)	S25	3.399(4)		
S3	3.300(4)	S20	3.371(4)	S16	3.401(4)		
S13	3.352(4)			S9	3.442(4)		
As2–		As3–		As4–		As5–	
S23	2.251(4)	S9	2.247(4)	S1	2.239(4)	S25	2.262(4)
S26	2.299(4)	S7	2.257(4)	S26	2.292(4)	S16	2.282(4)
S22	2.337(4)	S19	2.319(4)	S19	2.334(4)	S15	2.306(4)
S11	2.911(4)	S16	3.189(4)	S23	3.103(5)	S8	3.065(4)
S22	3.340(4)	S26	3.334(5)	S4	3.358(4)	S6	3.234(4)
As6–		As7–		As8–		As9–	
S4	2.243(4)	S12	2.230(4)	S6	2.317(4)	S18	2.239(4)
S10	2.257(4)	S13	2.233(4)	S22	2.335(4)	S21	2.281(4)
S14	2.314(4)	S17	2.332(4)	S11	2.572(4)	S17	2.322(4)
S27	3.172(5)	S15	3.183(4)	S4	2.629(4)	S24	3.075(4)

As10–		As11–		As12–		As13–		As14–	
S24	2.269(5)	S11	2.257(4)	S3	2.252(4)	S2	2.255(4)	S5	2.209(4)
S20	2.310(4)	S6	2.342(4)	S27	2.256(4)	S16	2.324(4)	S8	2.340(4)
S21	2.352(4)	S23	2.359(4)	S14	2.319(4)	S15	2.392(4)	S20	2.392(4)
S5	3.025(4)	S9	2.983(4)	S24	3.229(5)	S9	2.967(4)	S15	3.238(4)
S20	3.375(5)	S25	3.264(5)	S15	3.664(4)	S13	3.028(4)	S21	3.389(5)

1981), like Pb and Tl, and even more Pb and As, it is impossible to rely upon bond valence calculations for resolving the stoichiometry of the site, either.

The Pb/Tl situation is reflected in full in Table 2, further Tables carry a simplified denomination of these sites.

Arsenic coordinations (3 short bonds to S) form As_mS_n groups and crankshaft chains. They are concentrated in arsenic-rich (0 0 1) slabs between zig-zag planes of Pb-prisms. In agreement with all the members of the sartorite homologous series (Makovicky, 1985), these slabs approximate (3 0 1) and (3 0 $\bar{1}$) slabs of the SnS-like archetype, and consist of tightly-bonded double-ribbons (fragments of double-layers) of cations and anions, separated by interspaces which accommodate lone electron pairs of (especially) arsenic. Only the coordination of As8 suggests a position-flipping character, indicated by very nearly equally long opposing As8–S11 and As8–S4 bonds.

On the level of a single atomic plane (one of the surfaces of diagonally placed, tightly bonded double ribbons which form the As-rich slabs and are situated between zig-zag layers of Pb prisms), which can be easily compared with such planes in other M-sartorites, the following crankshaft chains are discernable (Fig. 3).

A W-shaped chain which incorporates a mixed "As1"site as one of its apices and is formed by As7–As9–As10–(As, Pb)1–As12–As6; a diagonal chain formed by As11–As2–As4–As3; a cation pair As5–As13; and two unconnected polyhedra, As8 and As14. The W-shaped chain and the rest of groups occur in the other known M-sartorites with higher M values but new, entire chain-like configurations are added each time with increasing M value.

On the level of a tightly-bonded double-layer, the bonding situation is more complicated (Fig. 4): the two surfaces are connected by inversion on centers situated

Table 4. Polyhedron characteristics for atoms in heptasartorite.

Atom	1	2	3	4	5	6	7	8
Pb1	9	3.215	0.015	0.401	0.933	139.178	67.108	1.969
Pb2	8	3.133	0.037	0.313	0.918	128.776	53.743	1.910
Pb3	8	3.096	0.063	0.235	0.936	124.301	50.499	1.975
Me4	9	3.278	0.021	0.183	0.962	147.522	70.640	*1.348*
Pb5	9	3.167	0.020	0.128	0.929	133.061	63.838	1.740
Pb6	9	3.203	0.053	0.120	0.939	137.685	56.524	*1.381*
Pb7	9	3.195	0.023	0.207	0.890	136.614	65.290	1.735
As/Pb1	5	2.747	0.335	0.341	0.967	86.786	11.926	1.872
As2	5	2.761	0.273	0.636	0.940	88.198	13.263	2.963
As3	5	2.835	0.339	0.692	0.989	95.490	13.055	3.033
As4	5	2.778	0.334	0.657	0.991	89.808	12.360	2.948
As5	5	2.789	0.364	0.648	0.955	90.840	11.936	3.005
As6	5	2.771	0.249	0.654	0.981	89.143	13.844	3.064
As7	5	2.778	0.324	0.671	0.979	89.847	12.566	3.145
As8	5	2.812	0.429	0.591	0.939	93.156	10.989	2.537
As9	5	2.876	0.242	0.718	0.940	99.643	15.613	2.981
As10	5	2.826	0.389	0.668	0.937	94.507	11.949	2.805
As11	5	2.776	0.341	0.609	0.951	89.618	12.210	2.783
As12	5	2.949	0.434	0.748	0.927	107.378	12.576	2.981
As13	5	2.801	0.441	0.619	0.995	92.034	10.629	2.828
As14	5	3.056	0.552	0.762	0.978	119.519	11.066	2.772

(1) Coordination number, (2) radius r_s in Å of a circumscribed sphere, least-squares fitted to the coordination polyhedron, (3) volume distortion $\upsilon = [V(\text{ideal polyhedron}) - V(\text{real polyhedron})]/V(\text{ideal polyhedron})$; the ideal polyhedron has the same number of ligands, (4) "volume-based" eccentricity $ECC_V = 1 - [(r_s - \Delta)/r_s]^3$; Δ is the distance between the center of the sphere and the central atom in the polyhedron, (5) "volume-based" sphericity $SPH_V = 1 - 3\sigma_r r_s$; σ_r is a standard deviation of the radius r_s, (6) volume in Å^3 of the circumscribed sphere, (7) volume in Å^3 of coordination polyhedron, (8) bond-valence sum.

between the As10 sites of the W-chains, and between the As2 sites of the long chains. The As8 site from one surface has short As–S bonds to S6 and S11, both of which are tightly-bonded to As11 of the long chain on the opposite surface, and to S22, bonded to As2 of the same chain. Thus, in the tightly bonded double layer we have a crankshaft chain As_5S_9 with an incomplete cage-like end (As11–As8–As2).

The As14 cation, situated as the "independent polyhedron" mentioned above on one surface, shares S20 and S8 with the apical "As1" and As10 sites of the W-shaped chain situated "under it" on the opposing surface. In this way, it participates in an As_7S_{14} linear group spanning both surfaces. The As5–As13 pair is a part of this cluster by being connected to the Me1 polyhedron.

A review of displacement parameters of sulfur atoms reveals that most of the atoms with augmented beta values are concentrated around the mixed (As, Pb)1 position (the shortest observed bonds: As1–S8 2.466 Å; As1–S27 2.471 Å). These are the S24 and S27 sites, the S25 site (As1–S25 2.701 Å), not connected to As1 by a short bond but forming a part of the coordination sphere of it, and to a lesser degree also As10 and As14. The only other site with augmented displacement parameters is Pb2 in the column of Pb atoms, without one of normally nine sulfur ligands, and the S12 site connected to it (Pb2 shares S8, and S24 with (As, Pb)1). An especially high beta parameter is observed for the Pb7 position, without any obvious reason in its first-configuration sphere. However, Pb7 shares S11 with As8, which appears to alternate between bonding to S4 (average 2.629 Å) and to S11 (average 2.572 Å), while preserving the short bonds to S6 (2.317 Å) and S22 (2.335 Å). Obviously, this switching exerts influence on the bonding situation of Pb7. The geometry of the slab-after-slab [0 0 1] sequences of the two phases will be described later.

All three "most Tl-enriched" lead sites have similar environment: they are surrounded on both sides (along [1 0 0]) by diverging short S–As bonds and the (Tl, Pb) polyhedron is faced by a lone electron pair of the protruding As atom (Fig. 3). For example, the Pb4 polyhedron is flanked by As8 and As11, and faced by As2 from a diagonal crankshaft chain. Tl-enriched sites do not appear related to the S vacancy: it is Pb2 that (in a way) faces this vacancy.

Enneasartorite. The structure of enneasartorite contains 27 independent metal and 35 different sulfur sites. There are nine Pb sites from which only two appear without thallium, 15 As sites, two mixed (As, Pb) sites (see Table 6) and one split As site. The unit cell of enneasartorite is a supercell of the fundamental motif of the sartorite homologous series for the homologue order $N = 3$. The a parameter is nine times the typical 4.2 Å value of the sartorite subcell whereas the b and c parameters are typical parameters for the known $N = 3$ homologues (*e.g.*, guettardite and twinnite) (Figs. 5 and 6, Tables 5 and 9).

Berlepsch *et al.* (2003) solved and refined a commensurate ninefold sartorite superstructure with space group $P2_1/c$; $a = 37.71(2)$, $b = 7.898(3)$, $c = 20.106(8)$ Å,

Table 5. Crystal data and summary of parameters describing data collection and refinement for enneasartorite.

Crystal data			
Chemical formula	$Tl_6Pb_{32}As_{70}S_{140}$	Unit-cell parameters	
Crystal system	Monoclinic	a(Å)	37.612(6)
Space group	$P2_1/c$ (#14)	b(Å)	7.8777(12)
D_x (mg m^{-3})	*4.83*	c(Å)	20.071(3)
No. of reflections for cell param.	5424	β(°)	101.930(2)
μ (mm^{-1})	34.97	V(Å^3)	5818.6(5)
Crystal form	Irregular	Z	1
Crystal size (mm)	0.10 × 0.05 × 0.04	Crystal color	Gray metallic

Data collection	
T_{min}, T_{max}	0.12, 0.54
No. of measured reflections	48149
No. of independent reflections	8301
No. of observed reflections	5842
Criterion for observed reflections	$I > 2\sigma(I)$
R_{int}(%), $R_{(sigma)}$ (%)	12.78, 7.73
θ_{max}(°)	23.3
Range of h, k, l	$-41 \le h \le 41$, $-8 \le k \le 8$, $-22 \le l \le 22$

Refinement on F_o^2	
$R[F_o > 4\sigma(F_o)]$ (%)	6.46
$wR(F_o^2)$ (%)	15.55
S (GooF)	0.992
No. of reflections used in refinement	5862
No. of parameters refined	576
Weighting scheme	$a = 0.08$, $b = 0$, $w = 1/[\sigma^2(F_o^2) + (aP)^2 + bP]$ where $P = (F_o^2 + 2F_c^2)/3$
$(\Delta/\sigma)_{max}$	0.002
$\Delta\rho_{max}$ (e/Å^3)	4.53 (0.90 Å from Pb5)
$\Delta\rho_{min}$ (e/Å^3)	−2.36 (1.08 Å from As19)
Extinction coefficient	None
Source of atomic scattering factors	*International Tables for X-Ray Crystallography* (1992, Vol. C, Tables 4.2.6.8 and 6.1.1.4)

β = 101.993(7)°. This lattice is identical with the lattice found in our measurements (see above). The refined formula $Pb_8Tl_{1.5}As_{17.5}S_{35}$ in the publication by Berlepsch *et al.* (2003) compares very well with the empirical formula $Pb_{8.2}Tl_{1.4}As_{17.5}Sb_{0.5}S_{35}$ which they obtained from electron microprobe analyses. The latter, recalculated to the base of 140 S atoms *pfu*, reads as $Pb_{32.8}Tl_{5.6}As_{70}Sb_{2.0}S_{140}$ which is very close to the formula obtained on a new material in this publication. It also reveals the same substitution mechanisms. The refined structure has 35 S atoms *pfu* instead of the expected 36 S, derived from "ideal sartorite", $Pb_9As_{18}S_{36}$. Berlepsch *et al.* (2003) suggest that incorporation of Tl is substantial for the formation of superstructures in sartorites, whereas Topa *et al.* (2017) and our current publication refine further their suggestion by demonstrating in detail connections between Tl contents and charge compensation problems generated in the structure by anion vacancies.

The nine repetitions of the 4.2 Å subcell in the *c* superperiod of enneasartorite host several diagonally disposed crankshaft chains (Fig. 7) with only two partly substituted As-large cation sites (refined as Pb in Table 6); the large cation forms about 20–30 at% of the site occupancy. As the other members of the "M-sartorite" family, enneasartorite contains a W-shaped crankshaft chain As10–As8–As7–As/Pb5–As6–As4. The As6–As8 pair of arsenic atoms are facing one another by the sides which host their respective lone electron pairs, eliminating the intermediate sulfur site "S36", although it was refined with 7 at% occupancy. We consider this refinement result to be a proof of structure disorder, the additional "partly void" sulfur position being somewhere else, with the same small percentage.

On the same surface of the double-ribbon, on the As/Pb5 side, the W-chain is accompanied by a crankshaft chain As18–As2–As1–As3 whereas at the opposite side it is accompanied by a chain As14–As12–As11–split As9a/As9b site. The array of As coordinations is completed by a two-cation As15–As16 group with cations connected via short As–S bonds. This group is laterally accompanied by isolated As/Pb13 and As17 polyhedra (Fig. 7).

How are these configurations present on the two surfaces of double-ribbons interconnected (Fig. 8)? The As15 and As16 pair on one surface is connected via S2 to two interconnected As17 polyhedra which, in turn, are connected to an As15 and As16 pair on the opposing side of the double ribbon. An As_6S_{10} crankshaft chain composed of three pairs is formed. The As/Pb5 and As7 polyhedra of the W-chain connect via S17 and S21 to the split As9b position on the opposite face of the double

Table 6. Coordinates, occupancy factors and equivalent isotropic displacement parameters (in Å^2) of atoms in enneasartorite.

Atom	Label	sof	*x*	*y*	*z*	U_{eq}
Me1	Pb/Tl		0.11797(3)	0.06147(12)	0.31086(5)	0.0337(3)
Pb2	Pb		0.23114(3)	0.08339(13)	0.31049(6)	0.0404(3)
Pb3	Pb		0.34280(3)	0.40289(12)	0.81511(5)	0.0319(3)
Pb4	Pb		0.45346(3)	0.09380(12)	0.31488(6)	0.0375(3)
Pb5	Pb		0.43845(3)	0.64183(13)	0.18291(5)	0.0328(3)
Pb6	Pb/Tl		0.33040(3)	0.59513(11)	0.20619(5)	0.0294(3)
Pb7	Pb		0.21828(3)	0.58297(13)	0.20423(6)	0.0406(3)
Me8	Pb/Tl		0.89227(3)	0.07051(12)	0.29256(5)	0.0366(3)
Pb9	Pb		0.00528(3)	0.07623(12)	0.29515(5)	0.0348(3)
As1	As		0.14489(6)	0.8405(3)	0.50350(11)	0.0200(5)
As2	As		0.85868(6)	0.4962(3)	0.37897(11)	0.0188(5)
As3	As		0.23522(6)	0.8216(3)	0.48893(11)	0.0235(5)
As4	As		0.26668(6)	−0.0063(3)	0.13439(11)	0.0206(5)
As5a	As	0.688(7)	0.3681(5)	0.710(3)	−0.0031(8)	0.0237(19)
Pb5b	Pb	0.312(7)	0.3609(4)	0.710(2)	−0.0191(7)	0.0237(19)
As6	As		0.36124(7)	0.0228(3)	0.11982(11)	0.0249(6)
As7	As		0.46738(6)	0.7089(3)	0.01061(12)	0.0284(6)
As8	As		0.49742(6)	0.0361(3)	0.13254(11)	0.0219(5)
As9a	As	0.48(2)	0.4107(8)	0.323(3)	0.0202(11)	0.059(2)
As9b	As	0.52(2)	0.4164(7)	0.298(3)	0.0086(10)	0.059(2)
As10	As		0.40334(6)	0.5104(3)	0.36325(11)	0.0227(5)
As11	As		0.30869(6)	0.1857(3)	0.49206(10)	0.0187(5)
As12	As		0.28815(9)	0.5223(3)	0.38208(13)	0.0481(9)
As13	As	0.799(4)	0.20513(15)	0.1969(6)	0.5421(3)	0.0249(9)
Pb13	Pb	0.201(4)	0.1984(3)	0.2538(10)	0.5250(5)	0.0249(9)
As14	As		0.18087(6)	0.4818(3)	0.36851(11)	0.0188(5)
As15	As		0.07981(6)	0.1700(3)	0.49605(12)	0.0244(6)
As16	As		0.07532(7)	0.4962(3)	0.38612(11)	0.0301(6)
As17	As		0.01748(7)	0.8173(3)	0.47361(12)	0.0333(6)
As18	As		0.04375(6)	−0.0257(3)	0.13239(10)	0.0175(5)
S1	S		0.05925(15)	0.3548(6)	0.2860(3)	0.0189(12)
S2	S		0.06522(17)	−0.0464(7)	0.4181(3)	0.0304(15)
S3	S		0.89520(15)	0.2989(7)	0.4429(3)	0.0269(14)
S4	S		0.09458(15)	0.1465(6)	0.1533(3)	0.0198(12)
S5	S		0.17136(16)	0.3378(7)	0.2696(3)	0.0266(14)
S6	S		0.19418(15)	0.0069(7)	0.4293(3)	0.0212(13)
S7	S		0.19338(15)	0.6671(7)	0.5383(3)	0.0266(14)
S8	S		0.22459(16)	0.1699(7)	0.1607(3)	0.0244(13)
S9	S		0.28298(15)	0.3750(6)	0.2850(3)	0.0204(12)
S10	S		0.30201(17)	−0.0398(7)	0.4213(3)	0.0284(14)
S11	S		0.3239(2)	0.8182(8)	0.0641(3)	0.0420(18)
S12	S		0.31618(16)	0.1717(6)	0.1583(3)	0.0240(13)
S13	S		0.39194(16)	0.3540(7)	0.2686(3)	0.0269(14)
S14	S		0.40898(15)	0.4858(7)	−0.0746(3)	0.0216(13)
S15	S		0.42762(17)	0.8592(7)	0.0597(3)	0.0288(14)
S16	S		0.49944(17)	0.8807(7)	0.2270(3)	0.0301(15)
S17	S		0.47673(17)	0.4717(7)	0.0777(3)	0.0315(15)
S18	S		0.52127(17)	0.8504(7)	0.0663(3)	0.0264(14)
S19	S		0.55184(15)	0.1861(6)	0.1627(3)	0.0201(12)
S20	S		0.38457(15)	0.8825(7)	0.2155(3)	0.0225(13)
S21	S		0.37860(15)	0.4646(7)	0.0739(3)	0.0224(13)
S22	S		0.34816(16)	0.3426(6)	0.4427(3)	0.0241(13)
S23	S		0.35586(16)	0.6866(7)	0.3402(3)	0.0243(13)
S24	S		0.27774(15)	0.8475(7)	0.2333(3)	0.0241(13)
S25	S		0.25385(14)	0.0135(6)	0.5762(3)	0.0181(12)
S26	S		0.25859(15)	0.3409(7)	0.4412(3)	0.0234(13)
S27	S		0.22376(14)	0.6685(6)	0.3449(3)	0.0183(12)
S28	S		0.83760(15)	0.3517(7)	0.2827(3)	0.0201(12)
S29	S		0.15937(16)	0.0528(7)	0.5846(3)	0.0240(13)
S30	S		0.11949(16)	0.3148(7)	0.4434(3)	0.0253(13)
S31	S		0.86803(15)	0.1540(6)	0.1514(3)	0.0194(12)
S32	S		−0.05390(16)	0.3327(7)	0.2663(3)	0.0233(13)
S33	S		−0.02930(14)	−0.02930(14)	0.4274(2)	0.0161(12)
S34	S		0.03384(17)	0.3487(8)	0.4564(4)	0.0457(19)
S35	S		0.00337(15)	0.1617(6)	0.1549(3)	0.0188(12)
S36	S	0.07(2)	0.431(3)	0.181(12)	0.154(5)	0.04(4)

Table 7. Selected interatomic distances (Å) in enneasartorite.

Me1–		Pb2–		Pb3–		Pb4–		Pb5–		Pb6–		Pb7–		Me8–		Pb9–	
S32	3.148(6)	S5	2.997(6)	S13	3.016(6)	S13	3.087(6)	S20	2.946(6)	S23	2.758(6)	S27	2.868(6)	S31	2.868(6)	S35	2.881(6)
S1	3.164(5)	S8	3.043(6)	S14	3.041(5)	S16	3.093(6)	S16	2.958(6)	S24	2.936(6)	S24	3.024(6)	S28	3.001(6)	S32	2.973(6)
S4	3.174(6)	S6	3.058(7)	S10	3.068(7)	S14	3.106(7)	S15	2.966(6)	S20	3.025(6)	S28	3.032(6)	S32	3.014(6)	S1	3.021(5)
S5	3.185(6)	S9	3.123(6)	S9	3.108(5)	S18	3.121(6)	S19	3.064(6)	S13	3.056(6)	S5	3.086(6)	S5	3.068(6)	S32	3.079(6)
S28	3.217(6)	S24	3.170(6)	S12	3.154(6)	S17	3.182(6)	S17	3.096(7)	S9	3.140(6)	S9	3.099(5)	S1	3.144(6)	S2	3.131(6)
S31	3.315(5)	S10	3.247(6)	S22	3.182(6)	S16	3.191(7)	S21	3.125(5)	S11	3.316(6)	S29	3.101(6)	S3	3.495(6)	S1	3.155(5)
S30	3.317(6)	S26	3.308(6)	S20	3.259(6)	S36	3.238(97)	S16	3.348(6)	S12	3.482(5)	S25	3.224(6)	S4	3.516(5)	S33	3.248(5)
S2	3.325(7)	S27	3.364(5)	S23	3.294(6)	S19	3.255(5)	S13	3.522(6)	S25	3.567(5)	S8	3.390(6)	S29	3.574(7)	S35	3.451(5)
S6	3.352(5)	S28	3.393(5)	S24	3.300(5)	S20	3.365(5)	S36	3.678(95)	S21	3.658(6)	S7	3.815(6)	S33	3.613(4)	S34	3.847(7)

As1–		As2–		As3–		As4–		As5a–		Pb5b–		As6–		As7–		As8–	
S7	2.270(6)	S28	2.242(6)	S6	2.276(6)	S8	2.249(7)	S21	2.455(22)	S11	2.532(17)	S20	2.232(6)	S15	2.284(7)	S16	2.245(6)
S3	2.304(7)	S3	2.285(6)	S25	2.310(6)	S24	2.258(6)	S11	2.497(21)	S10	2.653(15)	S11	2.274(7)	S17	2.288(6)	S18	2.282(7)
S29	2.319(6)	S4	2.320(6)	S7	2.363(7)	S12	2.301(6)	S15	2.611(19)	S21	2.674(16)	S12	2.321(7)	S18	2.380(6)	S19	2.332(6)
S6	2.918(7)	S7	3.097(7)	S27	3.079(6)	S11	3.129(8)	S14	2.908(22)	S23	2.907(16)	S36	2.857(7)	S14	3.047(6)	S36	2.859(**)
S2	3.254(6)	S8	3.359(6)	S10	3.280(7)	S7	3.275(6)	S10	2.953(19)	S14	2.909(17)	S15	3.255(7)	S17	3.335(7)	S15	3.063(6)
										S15	2.922(15)						
										S22	3.618(16)						

As9a–		As9b–		As10–		As11–		As12–		As13–		Pb13–		As14–		As15–	
S21	2.098(29)	S14	2.205(22)	S13	2.230(6)	S10	2.256(6)	S9	2.242(6)	S25	2.323(7)	S29	2.611(12)	S5	2.250(6)	S34	2.244(7)
S14	2.284(24)	S21	2.496(26)	S23	2.233(6)	S26	2.301(6)	S26	2.287(7)	S29	2.363(9)	S6	2.715(11)	S31	2.254(6)	S30	2.302(7)
S17	2.773(27)	S17	2.765(24)	S19	2.322(6)	S22	2.307(7)	S27	2.646(6)	S8	2.566(8)	S8	2.764(11)	S27	2.304(6)	S2	2.302(6)
S22	2.853(26)	S22	2.857(24)	S22	3.157(7)	S21	3.038(6)	S22	2.728(6)	S6	2.674(8)	S25	2.847(11)	S26	3.185(6)	S33	2.986(6)
S36	2.863(99)	S36	3.001(24)	S18	3.158(6)	S25	3.223(6)	S23	3.123(7)	S26	3.334(9)	S30	3.116(12)	S30	3.279(7)	S29	3.281(6)
												S26	3.162(13)				
												S7	3.275(10)				

As16–		As17–		As18–	
S1	2.268(6)	S33	2.301(5)	S35	2.230(6)
S30	2.310(6)	S33	2.431(5)	S32	2.281(6)
S34	2.585(8)	S2	2.539(7)	S4	2.311(6)
S31	2.705(6)	S35	2.817(6)	S34	3.244(6)
S35	3.183(6)	S34	2.921(8)	S3	3.302(7)

** occupancy of S36 is 7%.

ribbon. The latter is a beginning of the chain which ends with As14. The complete cluster contains 10 cations. The As/Pb13 site connects with the As3–As1–As2–As18 chain via S25 and S29, resulting in an As_5S_9 crankshaft chain. The W chains on the opposite faces of the double ribbon are displaced against one another by 4.2 Å (in the sense opposing the trend defined by the β angle) and they are related via the 2_1 axis of symmetry.

In all investigated structures of sartorite homologues, the non-bonding "lone" electron pairs of arsenic are primarily oriented into interspaces between the arsenic-rich double ribbons. Makovicky (1997) defined such arrangements as lone electron pair micelles, with non-bonded lone electron pairs oriented into, and concentrated in, centers (cores) of these arrangements, and with the cation–anion bonds which incorporate the lone electron pair micelle into, and interconnect it with, the crystal structure, oriented outwards. They envelope the core. The interspaces between double-ribbons are *primary lone electron micelle cores.* They are accompanied by *secondary lone electron pair micelles* in the surfaces of double ribbons because the orientation of lone pairs is diagonal to the ribbon surface, not perpendicular to it. These "secondary" interspaces, bridged only by weak interactions in the interior of the double ribbon (Fig. 7), are the means of adjusting the spacing of the As-rich portions to the periodicity required by columns of trigonal coordination prisms of lead in the structure. Projection of a tightly-bonded double-ribbon (Fig. 8) shows that in enneasartorite these secondary micelles represent two large V-shaped interspaces and one diagonally oriented simple interspace between adjacent crankshaft chains. Importantly, these interspaces stretch across the thickness of the double ribbon (Fig. 8) so that any adjustment of spacing in them can proceed unhindered. This scheme appears unique for the M-sartorite family of As-rich sartorite homologues, creating the M-fold superstructures in the process. In guettardite and twinnite, the partial antimony substitution for As, and in the $N=4$ homologues presence of more substantial concentrations of Pb or Ag in the ribbons, lead to 2×4.2 Å structures. The simple doubling of the 4.2 Å period is inevitable because of accommodation of coordination trapezoids of As(Sb).

Table 8. Polyhedron characteristics for atoms in enneasartorite.

Atom	1	2	3	4	5	6	7	8
Me1	0	3.247	0.017	0.111	0.976	143.332	68.912	1.409
Pb2	0	3.186	0.019	0.126	0.890	135.460	65.006	1.710
Pb3	0	3.152	0.017	0.117	0.930	131.158	63.086	1.806
Pb4	0	3.178	0.015	0.110	0.949	134.405	64.796	1.544
Pb5	0	3.154	0.021	0.329	0.896	131.416	62.960	1.924
Pb6	0	3.206	0.012	0.385	0.939	138.086	66.752	1.978
Pb7	0	3.177	0.037	0.278	0.812	134.258	63.254	1.958
Me8	0	3.248	0.019	0.369	0.962	143.579	68.942	1.722
Pb9	0	3.188	0.039	0.288	0.797	135.711	63.825	1.919
As1	0	2.729	0.258	0.608	0.952	85.123	13.059	2.951
As2	0	2.775	0.344	0.658	0.986	89.502	12.140	2.990
As3	0	2.788	0.340	0.619	0.953	90.789	12.385	2.761
As4	0	2.755	0.259	0.645	0.977	87.567	13.418	3.091
As5a	0	2.779	0.343	0.403	0.970	89.892	12.203	1.832
Pb5b	0	2.898	0.073	0.415	0.774	101.943	35.771	3.415
As6	0	2.673	0.372	0.592	0.845	79.957	10.380	3.157
As7	0	2.811	0.362	0.653	0.959	93.083	12.285	2.761
As8	0	2.598	0.299	0.512	0.874	73.483	10.654	3.119
As9a	0	2.812	0.460	0.654	0.900	93.152	10.401	3.134
As9b	0	2.812	0.460	0.499	0.900	93.152	10.401	2.278
As10	0	2.747	0.309	0.656	0.985	86.867	12.415	3.183
As11	0	2.770	0.350	0.639	0.958	89.047	11.975	2.983
As12	0	2.775	0.423	0.578	0.977	89.471	10.675	2.711
Pb13	0	2.965	0.123	0.341	0.910	109.216	36.228	3.046
As13	0	2.848	0.440	0.606	0.938	96.747	11.206	2.419
As14	0	2.813	0.337	0.685	0.962	93.269	12.790	3.077
As15	0	2.753	0.273	0.631	0.967	87.413	13.146	3.033
As16	0	2.772	0.376	0.588	0.950	89.217	11.506	2.651
As17	0	2.747	0.380	0.487	0.976	86.858	11.143	2.385
As18	0	2.818	0.298	0.682	0.996	93.776	13.617	3.030

(1) Coordination number, (2) radius r_s in Å of a circumscribed sphere, least-squares fitted to the coordination polyhedron, (3) volume distortion $\upsilon = [V(\text{ideal polyhedron}) - V(\text{real polyhedron})]/V(\text{ideal polyhedron})$; the ideal polyhedron has the same number of ligands, (4) "volume-based" eccentricity $ECC_V = 1 - [(r_s - \Delta)/r_s]^3$; Δ is the distance between the center of the sphere and the central atom in the polyhedron, (5) "volume-based" sphericity $SPH_V = 1 - 3\sigma_r r_s$; σ_r is a standard deviation of the radius r_s, (6) volume in Å^3 of the circumscribed sphere, (7) volume in Å^3 of coordination polyhedron, (8) bond-valence sum.

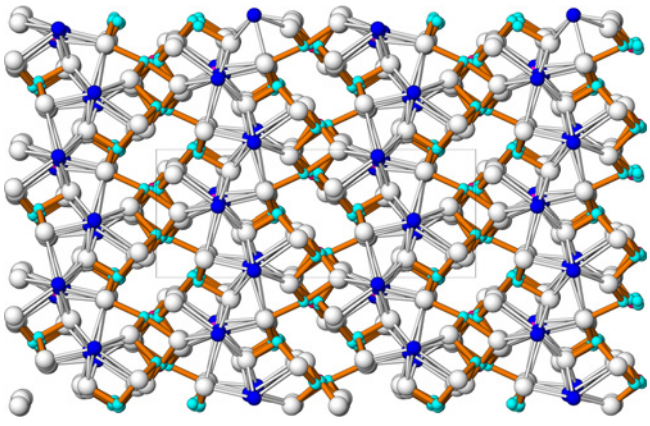

Fig. 1. The crystal structure of heptasartorite in projection parallel to [1 0 0]. In the order of decreasing size, spheres represent S (white), Pb (blue), Tl and (Tl, Pb) (mauve), and As (turquoise). There are seven subperiods projected in the direction of view. A zig-zag scheme of tightly-bonded double-ribbons (layer fragments) is recognizable especially in the As-rich structure portions (short As–S bonds in light brown).

As expectable, the refined positions of sulfur ligands around the mixed sites As/Pb5 and As/Pb13 are averages of positional/bond-length values required by respectively As and Pb, statistically occupying these cation sites, so that the bond length values calculated for these sites are not pure values. Problems connected with an incomplete separation of the two components, As9a and As9b, in the same coordination polyhedron are reflected in the calculated bond distances and equivalent displacement parameters (Tables 6 and 7).

There are two conspicuously large coordination polyhedra (trigonal tricapped prisms) among the string of "Pb" atoms in enneasartorite: *Me1* and *Me8* with the radius of the circumscribed sphere equal to ~3.25 Å; the former also has a conspicuously low BV equal to 1.4 valence units (Table 8). They occur on both sides of the Pb9 string which is parallel to the *b* direction. The previously outlined calculations indicate 43.8 at%Tl and 56.2 at% Pb for the *Me1* site, and 44.6 at% Tl and 55.4 at% Pb for the *Me8* site; they are the most preferred location of Tl in the structure (Fig. 7). Involvement of Pb6 with r_{sph}

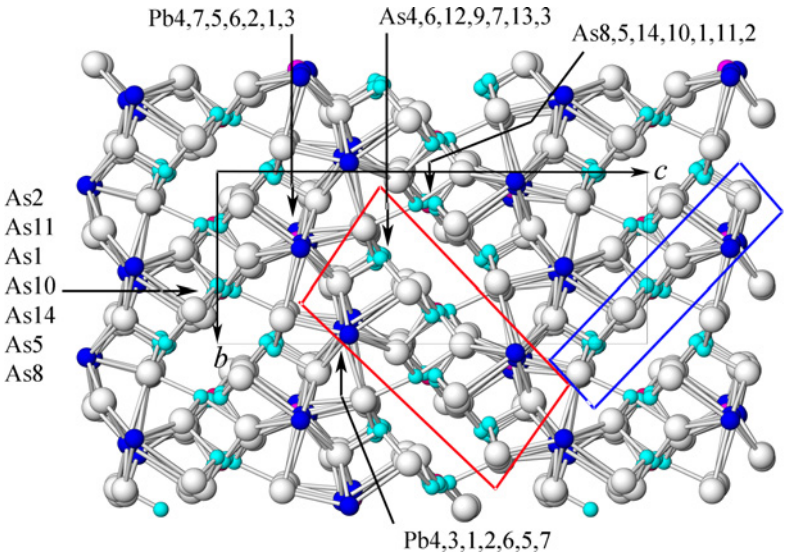

Fig. 2. Selected labels and other details in the crystal structure of heptasartorite. Sequences of cations in selected [1 0 0] columns in a unit cell are given and edge-on projections of single- and double-layers are indicated by frames. The blue frame relates to Fig. 3, red frame to Fig. 4.

Table 9. Comparative data for heptasartorite, enneasartorite, and related sartorite homologues with $N = 3$.

Mineral	Heptasartorite	Enneasartorite	9-fold sartorite	Sartorite subcell[§]	Guettardite	Twinnite
Formula	$Tl_7Pb_{22}As_{55}S_{108}$	$Tl_6Pb_{32}As_{70}S_{140}$	$Tl_6Pb_{32}As_{70}S_{140}$	$Pb_4As_8S_{16}$	$Pb_8As_8Sb_8S_{32}$	$Pb_{6.4}Tl_{0.8}Sb_{10.4}As_{6.4}S_{32}$
Crystal system	Monoclinic	Monoclinic	Monoclinic	Monoclinic	Monoclinic	Monoclinic
Space group	$P2_1/c$	$P2_1/c$	$P2_1/c$	$P2_1/c$	$P2_1/c$	$P2_1/n$
Cell parameters (Å)						
a	29.269(2)	37.612(6)	37.71(2)	4.19	8.527(4)	7.997(2)
b	7.8768(5)	7.877(1)	7.898(3)	7.89	7.971(4)	19.517(5)
c	20.128(2)	20.071(3)	20.106(8)	20.06	20.102(10)	8.634(2)
β(°)	102.065(2)	101.930(2)	101.993(7)	102.06	101.814(7)	91.061(4)
V(Å^3)	4537.8(5)	5818.6(15)	5857.5(35)	648.6	1337.3(11)	1347.4(6)
Z	1	1	1	1	1	1
Ref.[*]	1	1	2	3	4	5

[*] 1: This study; 2: Berlepsch *et al.* (2003); 3: Nowacki *et al.* (1961); 4: Makovicky *et al.* (2012); 5: Makovicky & Topa (2012).
[§] Transformed from Nowacki's subcell: $a = 19.62$, $b = 7.89$, $c = 4.19$ Å, $\alpha = \beta = \gamma = 90°$, monoclinic, space group $P2_1/n$ by the transformation matrix $R = [1\,0\,1,\ 0\,\bar{1}\,0,\ 0\,0\,\bar{1}]$.

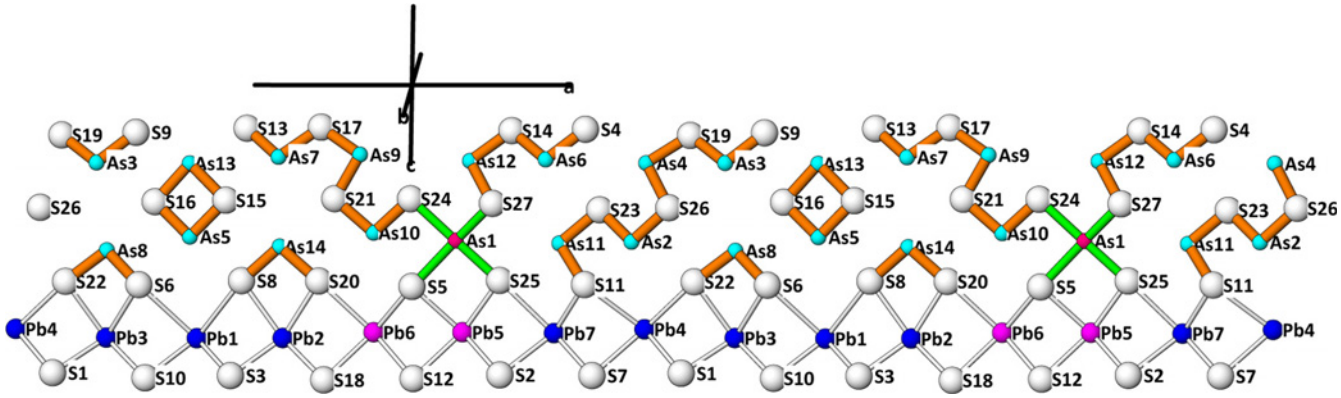

Fig. 3. A single atomic layer (a surface of a tightly-bonded double ribbon, see Fig. 2) from the crystal structure of heptasartorite with 2D crank-shaft chains, cation pairs and isolated coordination polyhedra of (preferably) As atoms indicated by short As–S bonds (coloured).

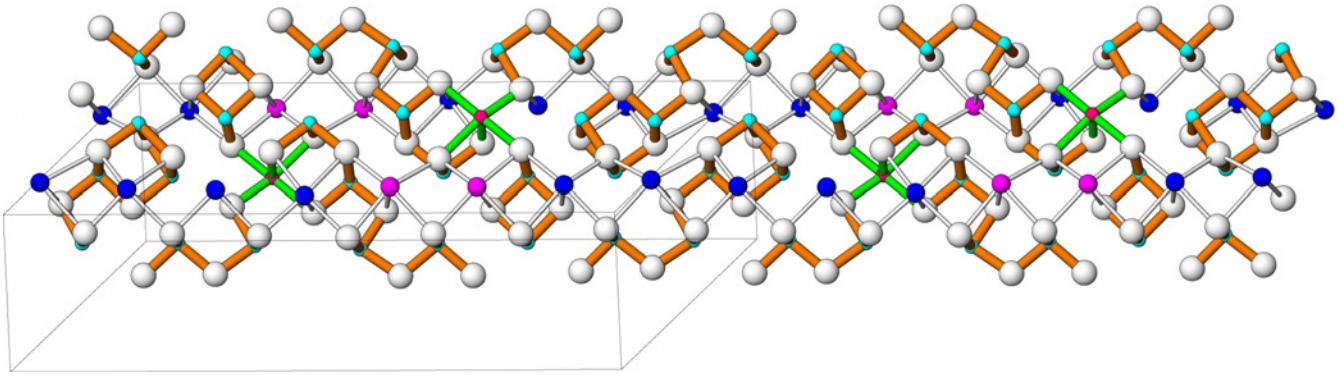

Fig. 4. A tightly-bonded double ribbon from the crystal structure of heptasartorite illustrating a 3D-crankshaft chain arrangement (compare with Fig. 3). Figs. 3 and 4 also illustrate the distribution of strongly-bonded groups and of the weakly bonded interspaces between them, as developed within the bounds of a double ribbon.

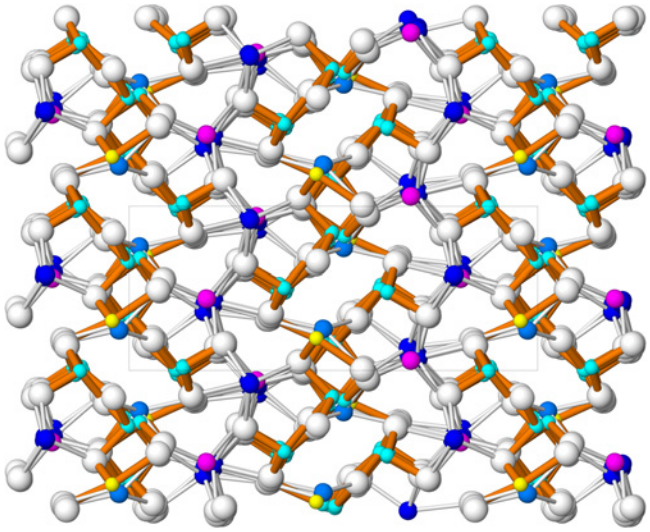

Fig. 5. The crystal structure of enneasartorite in projection parallel to [1 0 0]. In the order of decreasing size, spheres represent S (white), Pb (blue), Tl and (Tl, Pb) (mauve), (As, Pb) (yellow), and As (turquoise). There are nine subperiods projected in the direction of view. A zig-zag scheme of tightly-bonded double-ribbons (layer fragments) is recognizable especially in the As-rich structure portions (short As–S bonds indicated in light brown).

~3.21 Å, gives 26.2 at% Tl in this site, and the average Tl content for the four next larger sites (Pb2, 4, 7, 9) is calculated as 15.8 at%Tl in each. Altogether, this accounts for 81.2% Tl in the structure. With the semiquantitative character of these calculations as a warning, the rest of ~19% Tl has to be accommodated in the Pb3, Pb5 and the two mixed As/Pb5 and As/Pb13 sites (Table 7).

The nearly empty S36 site is 3.26 Å away from the Pb4 site and 3.68 Å from the nearby Pb5 site. Similar to the Tl sites, it occupies structure portions close to an inversion center. Sulfur vacancy and the Tl enriched site are not tied to one another. Across the Pb layer, the vacant S36–S36 sites are separated by a shift of $1\frac{1}{2} \times 4.2$ Å interval whereas the Tl-rich groups are separated by a $2\frac{1}{2} \times 4.2$ Å interval.

In general features, the crystal structure of *hendekasartorite*, not described in detail here, is another typical structure of the $N = 3$ member of the sartorite homologous series, similar to those of hepta- and enneasartorite. A principal property of the structure is the positional modulation of arsenic sites along the 11×4.2 Å *a* direction, as a further development of the structures described here. So far it is the longest modulated direction among M-sartorite structures with a complete structure refinement.

4. Analogies and differences between the structures of M-sartorites

Concerning connectivity, the W chain in heptasartorite (Fig. 4) has a single V shaped coordination attached to it from the opposite side of the double ribbon. In the enneasartorite (Fig. 8), the arrangement is different: the apical attachment on the other face of the double ribbon is a part of the As14–As9b crankshaft chain.

The single diagonal chain with a cage-like end (via a V-shaped group attached) in heptasartorite has full analogy in enneasartorite. An "interconnected chain" occupies both surfaces of the double-ribbon in the enneasartorite structure; its two portions are interconnected via an As17–As17 configuration. As15 & As16 in enneasartorite form on the surface an As_2S_2 group which in this phase is not independent. It is interconnected through the ribbon thickness with other configurations. It is quasi-independent, connected only with the mixed (As, Pb)1 polyhedron, when it occurs as the As5 and As13 pair in heptasartorite (Fig. 4).

What concerns the independent three-bonded As polyhedra on double-ribbon surfaces (Figs. 3 and 7), in heptasartorite it is As14 and As8. They either combine into a cage which terminates a chain, or form a cap on the W chain. In enneasartorite, As 17 and As13 respectively interconnect two partial chains or terminate a chain in a cage-like manner. As13 is a mixed site.

Slab-after-slab stacking reveals a complicated picture of inversions and shifts.

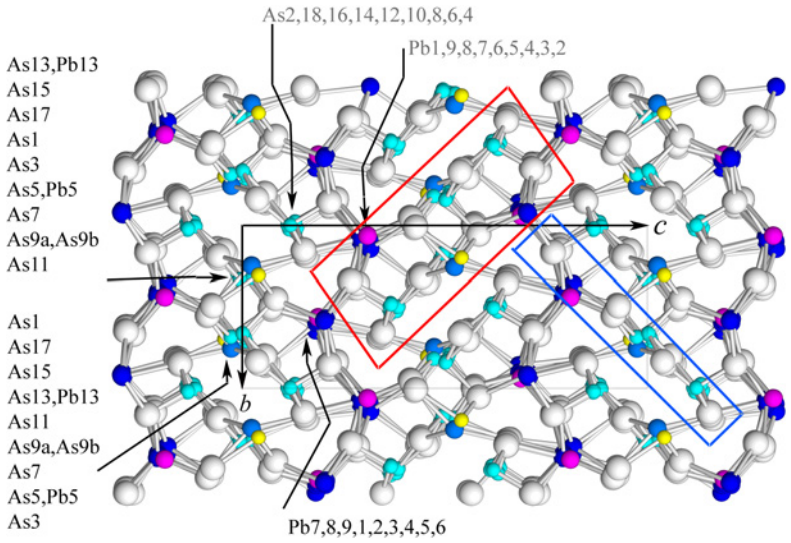

Fig. 6. Selected labels and other details in the crystal structure of enneasartorite (sequences of cations in selected [1 0 0] columns, edge-on projections of single- and double-layers). Blue frame relates to Fig. 7, red frame to Fig. 8.

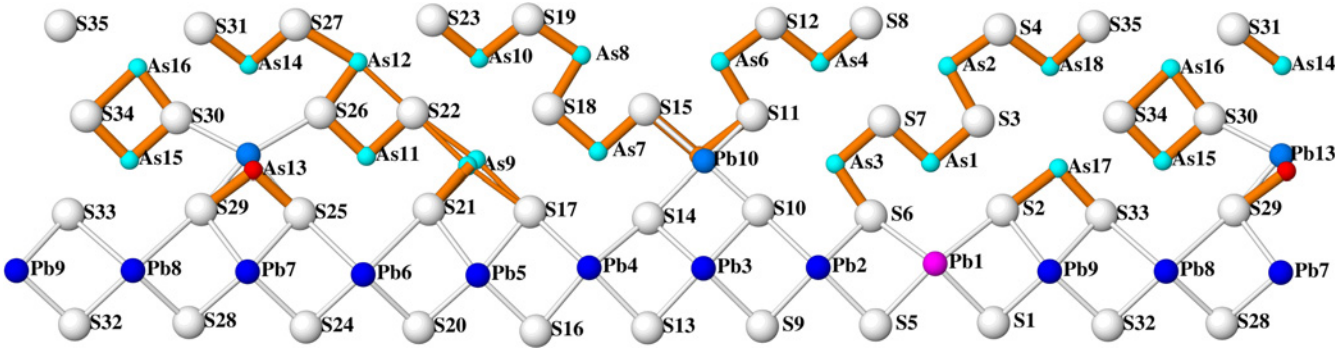

Fig. 7. A single atomic layer (a surface of a tightly-bonded double ribbon, see Fig. 6) from the crystal structure of enneasartorite with 2D crank-shaft chains, cation pairs and isolated coordination polyhedra of (preferably) As atoms as defined by short As–S bonds. Note the missing "S36" position in the sequence of marginal S atoms. As an example of the secondary lone electron pair micelle we can quote the S14–S23–S27 interval between chains and groups into which the lone electron pairs of As7, 9, 10, and 12 are partly oriented.

Heptasartorite. When we examine the slab-after-slab [0 0 1] sequence, the stacking shift of glide-reflected equivalent cation and anion sites is ½ [1 0 0] *subperiod* of 4.2 Å per slab thickness. Double-ribbons contain inversion centers and Pb prismatic walls contain two-fold screw axes. The minimum shift of equivalent (inverted) elements on the opposite sides of the same slab (Fig. 4) is 1/2 *subperiod* (there is an inversion center between them), and a pair of vacancies across the Pb plane is one 4.2 Å subperiod in the a × c plane.

Enneasartorite. The practically missing S36 site is 3.26 Å away from the Pb4 site and 3.68 Å from the nearby Pb5 site. It occupies structure portions close to 2_1 axes so that the inverted anion vacancies are spaced by one subperiod across the Pb slab. The glide-reflected groups in two adjacent slabs are mutually spaced by ½ of the 4.2 Å subperiod across the Pb-slab, creating the β angle of the lattice (Fig. 9).

In the studied structurally ordered hendekasartorite structure (in preparation), slab shifts in the layer *stack* along the [0 0 1] direction represent a shift of two and a half 4.2 Å subperiods for the positional difference between the glide-plane related slab configurations in two adjacent slabs. This is very different from hepta- and enneasartorites in which this shift was ½ subperiod.

A permanent feature of M-sartorites is a mixed site in the "basis" of the W-shaped chain configuration, a neighbor to a pure As site (Figs. 3 and 7). In heptasartorite this site (As1) was refined as $As_{80}Pb_{0.20}$ with two shortest bonds equal to 2.466 Å and 2.474 Å, the rest being 2.702–2.848 Å. Radius of the circumscribed sphere, r_{sph} is 2.747 Å, eccentricity of the central atom modest (0.341), much less than the arsenic atoms in the structure (Table 4). Bond valence value, calculated for As, is only 1.87 what reflects the fact that even the shortest bonds of "As1" are too long for As, because the ligands in the coordination polyhedron represent averages of the ligand positions in the As-filled polyhedra and of the ligand positions in the much larger and differently shaped Pb (and perhaps also Tl, see above) polyhedra in the same site. The calculated bond valence value is a result of combined polyhedron sizes and shapes, not valencies.

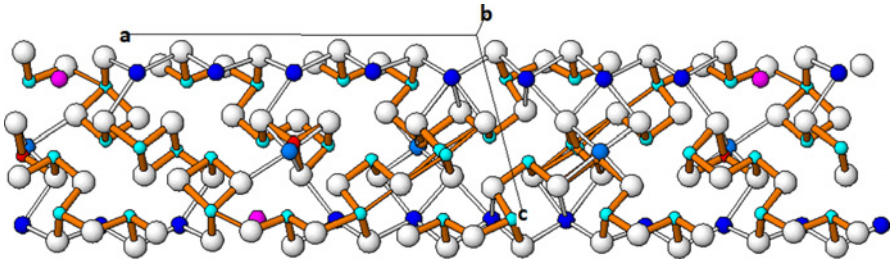

Fig. 8. A tightly-bonded double ribbon from the crystal structure of enneasartorite (inclined for clarity) to indicate a 3D-crankshaft chain arrangement (compare with Fig. 7). Figs. 7 and 8 also illustrate the distribution of strongly bonded groups, and of the weakly bonded interspaces between them, within the bounds of a double ribbon.

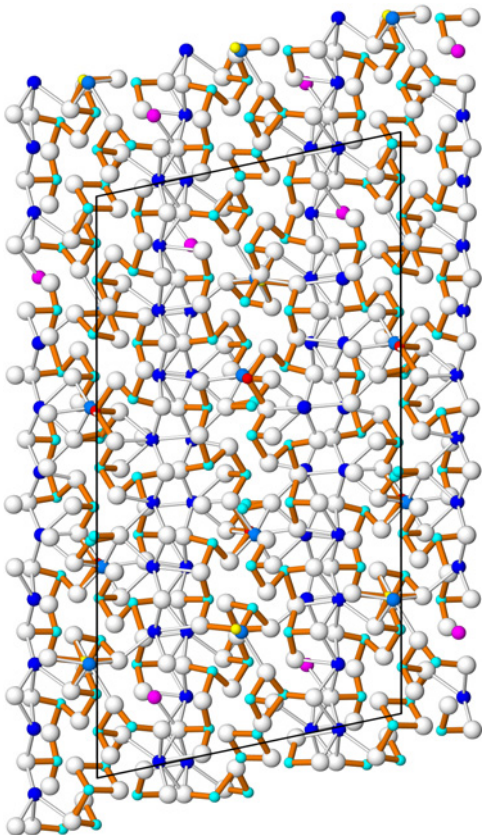

Fig. 9. The crystal structure of enneasartorite projected upon (0 1 0) in order to show reflections, inversions and shifts of prominent elements/groups within and across individual slabs of the structure. The elements shown in Figs. 7 and 8 are alternatively dipping below and surfacing above the projection plane when moving from left to right.

The same position in enneasartorite (As5) was refined as a split position $As_{0.69}Pb_{0.31}$ but the refinement appears indecisive (Tables 6 and 8, Fig. 7). The short bonds of the "As" component are 2.455–2.611 Å, the rest are 2.908–2.953 Å. The "Pb" component is not well separated, with "bond lenghts" 2.532–2.674 Å, and then 2.907 Å and above. Again, this reflects the "average character" of the ligand positions, averaged from those in the As and the Pb polyhedra. As a result, for the As component, radius r_{sph} is 2.799 Å, eccentricity 0.403, and bond valence only 1.8. The "Pb" component has similar values (Table 8), unusually high eccentricity 0.415 and formal bond valence equal to 3.4, because the averaged ligand positions are too close for a large cation, and not because of its true valence.

The As-predominant composition site "As15" in hendekasartorite, $As_{80}Pb_{0.20}$, has similar bonds and polyhedron properties (in prep.). In all three cases the volume of the circumscribed sphere to the mixed "As" polyhedron is modest, 86.8–89.9 $Å^3$, much less than that of the associated As polyhedra and reflects a lower lone electron pair activity than that of surrounding As atoms. The unity of design and occupation scheme in all three phases is apparent and important for interpretation.

Heptasartorite does not contain other mixed sites which involve arsenic. Enneasartorite (Table 6) has one more mixed site (0.799 As13 and 0.201 Pb13) figuring as one of the "independent" "AsS_3" sites, spaced nearly centrally between two Me5 sites. Hendekasartorite has four additional mixed sites. The near-central insertion of such sites between two adjacent mixed sites from the W-shaped chain in the latter two phases, apparently helps to maintain geometric stability of the slab interior in hendekasartorite. X-ray diffraction studies are not giving answer about possible Tl contents in all these sites but comparison of chemical and crystal structure data, performed above, makes presence of Tl probable.

5. Comparison with As–Sb containing $N = 3$ homologues

In the known cases of As–Sb containing $N = 3$ structures of the sartorite homologous series, only a doubling of the 4.2 Å axis is observed, contrary to the 7-fold and 9-fold superperiods observed in hepta- and enneasartorite. The crankshaft chains are in general diagonally oriented with different degree of clarity because of an ambiguously coordinated Sb (or Sb-rich) site in their centre (Fig. 10). Manifest switching of chain orientation, seen especially in enneasartorite, has not been observed.

In *guettardite*, $PbAsSbS_4$ (Makovicky *et al.*, 2012) (Table 9), the one-surface crankshaft chain is composed of the sequence As2(sof 1.05)–a typical flipping Sb2 (sof 0.94)–As1(sof 0.98), whereas the lone polyhedron is Sb1 (sof 0.98; the refined sof values express the weak Sb-As mixing in the sites) (Fig. 10). Size difference between the Pb1 and Pb2 polyhedra in the zig-zag walls of trigonal coordination prisms in guettardite is small; they both

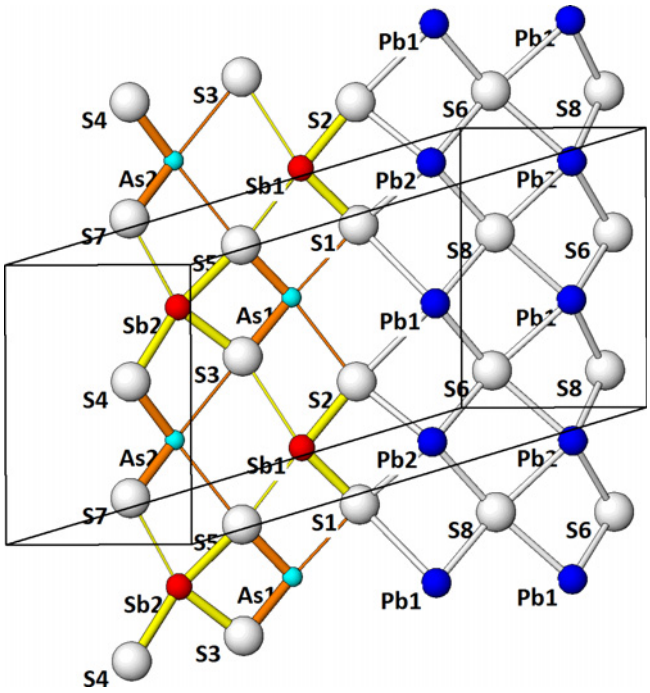

Fig. 10. A surface of a double ribbon from the crystal structure of guettardite, $PbAsSbS_4$, illustrating the shape and extent of crankshaft chains of As and Sb in the mixed As–Sb members of the sartorite homologous series. Bulk of colour scheme as in Fig. 5; Sb is coloured red with yellow Sb–S bonds.

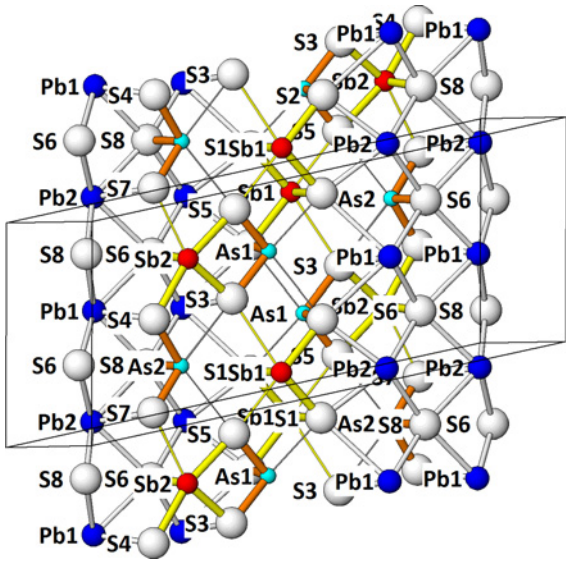

Fig. 11. Diagonal $As_4Sb_4S_{16}$ crank-shaft chains in the interior of a tightly-bonded double-ribbon in the structure of guettardite. Colour code as in Fig. 10.

adjust by distorting their ideal prismatic shape. In the related *twinnite*, $Pb_{0.8}Tl_{0.1}Sb_{1.3}As_{0.8}S_4$ (Makovicky & Topa, 2012), the chain starts with $(As_{0.62}Sb_{0.38})6$, continues via flipping bonds of the Sb4 site to the $(As_{0.87}Sb_{0.13})5$ site; the opposing sole polyhedron is Sb3. The shortest bonds of these Sb4, As5 and Sb3 sites correlate in their lengths in order to produce a narrow crankshaft chain in the double-ribbon surface. In both these sulfosalts the chains and groups on the opposing surfaces of a double-ribbon are interconnected into a complex crankshaft chain, *e.g.* $As_4Sb_4S_{16}$ in guettardite (Fig. 11).

The structure of Tl-rich $N=3$ homologue, *pierrotite*, $Tl_2(Sb,As)_{10}S_{16}$ (Engel *et al.*, 1983) represents a sort of compromise: on one face of a double-ribbon, two Sb and one As polyhedron form an "open" crankshaft chain which ends in a half-independent but not quite bond-wise separated, fourth Sb polyhedron; on the other face, a side-bonded As3 site is bond-wise separated from a As4–Sb3 pair which itself is separated from an independent side-bonded As1 polyhedron. Thus, the structure appears to unite (with some compromise) the two configurations.

Similar situation is observed in the $N=3$ slabs of the recently determined structures of the $N_{1,2}=3$; 4 homologues. The configurations in the $N=3$ slab of *écrinsite* structure (Topa *et al.*, 2017) tend towards bond topology similar to that of the $N=3$ slab in *guettardite and twinnite* (Makovicky *et al.*, 2012; Makovicky & Topa, 2012). In the surface of a tightly-bonded double ribbon, the marginal, side-bonded As3 site ($As_{0.82}Sb_{0.18}$) is followed in écrinsite by a flipping Sb1 site (100% Sb). The latter associates with the side-bonded As4 site via short bonds to S1 and S9. The Sb1–As4 distance is 3.45 Å and the latter group is almost symmetrical. The 2.85 Å Sb1–S distance is opposed by 2.60 Å in the pair, suggesting a weak amount of possible flipping of the Sb1 atom between two alternative bond schemes. This results in a (poorly defined) diagonally orientated three-cation crankshaft chain. This configuration is completed by a single Sb2 site. The large trigonal prism of Tl1 faces long As–S distances of the As4 polyhedron.

In the very similar structure of the type *boscardinite* (Orlandi *et al.*, 2012), the $N=3$ chain is composed of the Sb3 ($Sb_{0.71}As_{0.29}$)–Sb1–As4 ($As_{0.75}Sb_{0.25}$) polyhedra, and the opposing polyhedron is Sb2. However, here the flipping of the Sb1 site is more pronounced, the connection to the S atom in the Sb3 polyhedron is 2.77 Å, opposed by 2.67 Å in the Sb1–As4 pair. In the (Tl, As)-enriched boscardinite (Biagioni & Moëlo, 2017) the Sb3 site became an arsenic-dominated site, As3 ($As_{0.60}Sb_{0.40}$), and the bond (flipping) scheme of Sb1 approaches that in écrinsite.

The principal difference between these cases and the sartorite omission derivatives treated here is that in the Sb–As structures the crankshaft chain which starts by a side-bonded atom at the ribbon margin (Fig. 10) continues through two atoms (Sb and As–Sb sites in general) which tend to form a tight pair via more or less defined short bonding to two common S atoms. The fourth atom, which is situated in the chain direction, at the opposite margin of the ribbon, forms an isolated, independent Sb polyhedron, not sharing short Sb–S bonds with a chain on a surface of the double-ribbon. Except for an occurrence of a rare split

position at the end of the chain, the diagonal crankshaft chains in the sartorite omission derivatives (Figs. 3 and 7) do not close in a tightly-bonded cation pair but they are true "open" crankshafts in which the fourth cation is connected to the previous three cations of the chain by a short As–S bond, instead of being isolated.

On the one hand, introduction of Sb instead of a part of As makes a fit of the metalloid-rich structure portions with the Pb-rich ones easier to resolve, whereas on the other hand, it also allows formation of local configurations not usual in As-only homologues. These two factors combined cause the observed differences between the two groups of compounds and make the Sb-poor Lengenbach locality unique among the occurrences of the sartorite group minerals.

Acknowledgements: This project was supported by the University of Copenhagen, Naturhistorisches Museum Wien and Technische Universität Wien. Positive suggestions by the anonymous reviewers and assistance of the EJM editor, Prof. S.V. Krivovichev, are gratefully acknowledged.

References

Bannister, E.A., Pabst, A., Vaux, G. (1939): The crystallography of sartorite. *Mineral. Mag.*, **25**, 264–270.

Berlepsch, P., Armbruster, T., Makovicky, E., Topa, D. (2003): Another step toward understanding the true nature of sartorite: determination and refinement of a nine-fold superstructure. *Am. Mineral.*, **88**, 450–461.

Berry, L.G. (1940): Baumhauerite, rathite and sartorite. in "Roentgenographic observations on ore minerals". *Univ. Toronto Studies, Geol. Ser.*, **44**, 47–69.

Biagioni, C. & Moëlo, Y. (2017): Lead-antimony sulfosalts from Tuscany (Italy). XVIII. New data on the crystal-chemistry of boscardinite. *Mineral. Mag.*, **81**, 47–60.

Brown, I.D. (1981): The bond-valence method: an empirical approach to chemical structure and bonding. *in* "Structure and bonding in crystals", M. O'Keeffe & A. Navrotsky, eds. Academic Press, New York, 1–30.

Bruker A.X.S. (1997): XPREP, Version 5.1. Bruker AXS Inc., Madison, WI 53719, USA.

— (1998a): SMART, Version 5.0. Bruker AXS Inc., Madison, WI 53719, USA.

— (1998b): SAINT, Version 5.0. Bruker AXS Inc., Madison, WI 53719, USA.

Engel, P., Gostojic, M., Nowacki, W. (1983): The crystal structure of pierrotite, $Tl_2(Sb, As)_{10}S_{16}$. *Z. Kristallogr.*, **165**, 209–215.

Iitaka, Y. & Nowacki, W. (1961): Refinement of the pseudo crystal structure of scleroclase, $PbAs_2S_4$. *Acta Crystallogr.*, **14**, 1291–1292.

Laroussi, A., Moëlo, Y., Ohnenstetter, D., Ginderow, D. (1989): Argent et thallium dans les sulfosels de la série de la sartorite (Gisement de Lengenbach, vallée de Binn, Suisse). *Comptes Rendus Acad. Sci., Paris*, **308**, 927–933.

Le Bihan, M.-Th. (1962): Étude structurale de quelques sulfures de plomb et d'arsenic naturels du gisement de Binn. *Bull. Soc. Franç. Minéral. Cristallogr.*, **85**, 15–47.

Makovicky, E. (1985): The building principles and classification of sulphosalts based on the SnS archetype. *Fortschr. Mineral.*, **63**, 45–89.

— (1997): Modular crystal chemistry of sulphosalts and other complex sulphides. *EMU Notes Miner.*, **1**, 237–271.

Makovicky, E. & Topa, D. (2012): Twinnite, $Pb_{0.8}Tl_{0.1}Sb_{1.3}As_{0.80}S_4$, the OD character and the question of its polytypism. *Z. Kristallogr.*, **227**, 468–475.

Makovicky, E., Topa, D., Tajjedin, H., Rastad, E., Yaghubpur, A. (2012): The crystal structure of guettardite, $PbAsSbS_4$. *Can. Mineral.*, **50**, 253–265.

Nowacki, W. & Bahezre, C. (1963): Die Bestimmung der chemischen Zusammensetzung einiger Sulfosalze aus dem Lengenbach (Binnatal, Kt. Wallis) mit Hilfe der elektronischen Mikrosonde. *Schweiz. Miner. Petrogr. Mitt.*, **43**, 407–411.

Nowacki, W., Iitaka, Y., Buerki, H., Kunz, V. (1961): Structural investigations on sulfosalts from the Lengenbach, Binn Valley (Ct. Wallis). Part II. *Schweiz. Miner. Petrogr. Mitt.*, **41**, 103–116.

Nowacki, W., Marumo, F., Takeuchi, Y. (1963): Untersuchungen an Sulfiden aus dem Binnatal (Kt. Wallis, Schweiz). *Schweiz. Miner. Petrogr. Mitt.*, **44**, 5–9.

Orlandi, P., Biagioni, C., Bonaccorsi, E., Moëlo, Y., Paar, W.H. (2012): Lead-antimony sulfosalts from Tuscany (Italy). XII. Boscardinite, $TlPb_3(Sb_7As_2)_{\Sigma 9}S_{18}$, a new mineral species from the Monte Arsiccio mine: occurrence and crystal structure. *Can. Mineral.*, **50**, 235–251

Pring, A. (2001): The crystal chemistry of the sartorite group minerals from Lengenbach Binntal, Switzerland – a HRTEM study. *Schweiz. Miner. Petrogr. Mitt.*, **81**, 69–87.

Pring, A., Williams, T., Withers, R. (1993): Structural modulation in sartorite: an electron microscopy study. *Am. Miner.*, **78**, 619–626.

Sheldrick, G.M. (2008): A short history of *SHELX*. *Acta Crystallogr.*, **A64**, 112–122.

Topa, D., Makovicky, E., Berlepsch, P., Stoeger, B., Stanley, C. (2015): IMA No. 2015-075 Hendekasartorite $Tl_2Pb_{48}As_{82}S_{172}$, Lengenbach quarry, Binntal, Wallis, Switzerland.

Topa, D., Makovicky, E., Stoeger, B., Stanley, C. (2017): Heptasartorite, $Tl_7Pb_{22}As_{55}S_{108}$, enneasartorite, $Tl_6Pb_{32}As_{70}S_{140}$, and hendekasartorite, $Tl_2Pb_{48}As_{82}S_{172}$, three members of the anion-omission series of 'sartorites' from the Lengenbach quarry at Binntal, Wallis, Switzerland. *Eur. J. Mineral.*, **29**, 701–712.

Received 24 February 2017
Modified version received 28 April 2017
Accepted 16 May 2017